ACS APPLIED MATERIALS & INTERFACES

Letter

www.acsami.org

Intertwined Network of Si/C Nanocables and Carbon Nanotubes as Lithium-Ion Battery Anodes

Bin Wang,[†] Xianglong Li,*[,†] Bin Luo,[†] Xianfeng Zhang,[†] Yuanyuan Shang,[‡] Anyuan Cao,[‡] and Linjie Zhi*[,†]

[†]National Center for Nanoscience and Technology, Beijing 100190, P. R. China

[‡]Department of Materials Science and Engineering, College of Engineering, Peking University, Beijing 100871, P. R. China

Supporting Information

ABSTRACT: We demonstrate a new kind of Si-based anode architectures consisting of silicon nanowire/overlapped graphene sheet core–sheath nanocables (SiNW@G) intertwined with carbon nanotubes (CNTs). In such a hybrid structure, the CNTs, mechanically binding SiNW@G nanocables together, act as a buffer matrix to accommodate the volume change of SiNW@G, and overlapped graphene sheets (that is, G sheaths) effectively prevent the direct contact of silicon with the electrolyte during cycling, both of which enable the structural integrity and interfacial stabilization of such hybrid electrodes. Furthermore, the one-dimensional nature of both components affords the creation of a three-dimensional interpenetrating network of lithium ion and electron pathways in the resultant hybrids, thereby enabling efficient transport of both electrons and lithium ions upon charging/discharging. As a result, the hybrids exhibit much-improved lithium storage performance.

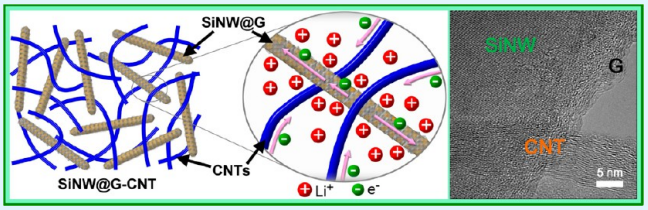

KEYWORDS: *carbon nanotubes, silicon nanowires, graphene, nanocables, lithium-ion batteries*

1. INTRODUCTION

The ever growing demand for energy storage has sparked a great interest in the development of high energy and power density lithium-ion batteries (LIBs).[1−5] The development of electrode materials and architectures is crucial for the improvement of the electrochemical performances of such battery systems. Among various anode materials investigated so far, silicon (Si) has attracted considerable attention because of its abundance in nature, appropriately low working potential, and more importantly, the highest known theoretical specific capacity of ∼4200 mA h g^{-1} which is more than ten times higher than that of commercialized graphite (372 mA h g^{-1}).[6−13] However, silicon experiences a dramatic volume change (>300%) during the charge–discharge processes.[14] This change not only causes severe pulverization and electrical disconnection from the current collector, it also induces continual formation of so-called solid electrolyte interphase (SEI) on the silicon surfaces newly exposed to the electrolyte,[15] both of which result in the performance degradation of silicon. As the nanostructuring of Si, for example, the construction of Si nanowires (SiNWs),[4] can improve its mechanical integrity during charge–discharge cycling, the shielding of nanostructured Si with a second phase (e.g., C) is considered one of the most promising strategies for simultaneously dealing with the structural and interfacial stability issues of Si. Notably, the thus-hybridized anode materials also afford short electron and lithium ion transport lengths, which are highly favorable for improving their rate capability and hence power density. Accordingly, diverse Si/C hybrid anode materials have recently been proposed, some of which include C-coated Si nanoparticles,[16,17] C-sheathed Si nanowires,[18−22] C-covered Si nanotubes,[23−25] and C-sandwiched Si nanomembranes.[26] However, to fully exert their advantages, these nanoscale hybrid anode materials must then be elaborated into an electrode architecture that is capable of accommodating the volume change of Si, providing electrical contacts to each Si/C hybrid unit, and maintaining the short lithium ion diffusion and transport length. While the conventional electrode configuration with conductive additives and polymer binders adversely affects the designated performances of the nanomaterials,[27] the direct integration of these nanoscale hybrid materials units as an array on the current collectors is an attractive and efficient approach to enable the exertion of such hybrid nanomaterials as LIB anodes.[20,22] Yet, the introduction of heavy current collectors (e.g., stainless steel substrates) can substantially dilute the performance provided that all the electrode components have to be counted for practical applications.

As an alternative, Si/C hybrid nanomaterials can be engineered into a lightweight, robust, and flexible matrix (e.g., graphene or reduced graphene oxide (RGO),[28−30] or carbon nanotubes (CNTs)[31,32]), which holds the ability to mechan-

Received: May 27, 2013
Accepted: June 28, 2013
Published: June 28, 2013

ically and electrically bind these nanoscale hybrid materials units together, thereby forming a functional LIB anode. As an example, we recently demonstrated a kind of self-supported binder-free Si-based anodes (namely, SiNW@G@RGO) consisting of silicon nanowire/overlapped graphene sheet core−sheath nanocables (SiNW@G) sandwiched in between RGO, and showed their remarkable lithium storage performances as well.[33] In such a unique anode structure, the overlapped graphene sheets, as adaptable but sealed sheaths, prevent the direct exposure of encapsulated silicon to the electrolyte and enable the structural and interfacial stabilization of silicon nanowires. Meanwhile, the flexible and conductive RGO overcoats accommodate the volume change of embedded nanocables and thus maintain the structural and electrical integrity of the SiNW@G@RGO throughout the whole electrode.

In this letter, we develop a new kind of Si-based anode architectures (namely, SiNW@G-CNT) consisting of SiNW@G nanocables intertwined with CNTs to promote the electrochemical performance of Si as an anode material of LIBs, especially high rate capability (Figure 1). Here, the

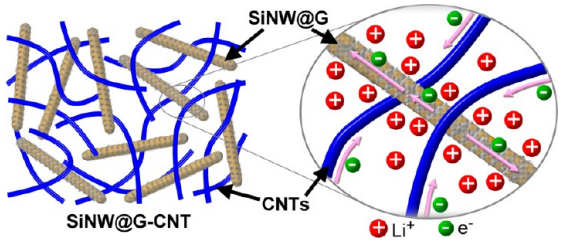

Figure 1. Schematic illustration of the 3D intertwined network of SiNW@G nanocables and CNTs, functioning as a LIB electrode with interpenetrating pathways for fast transport of both electrons and lithium ions.

CNTs, mechanically binding SiNW@G nanocables together, act as a buffer matrix to accommodate the volume change of SiNW@G, and overlapped graphene sheets (that is, G sheaths) alleviate the SEI formation and propagation on the SiNW surface during cycling, both of which enable the structural integrity and interfacial stabilization of such hybrid electrodes. More importantly, thanks to one-dimensional nature of both components, the hierarchical one-dimensional/one-dimensional (1D/1D) combination formula demonstrated creates a three-dimensional (3D) interpenetrating network[34,35] of lithium ion and electron pathways in the resultant hybrids, thereby enabling efficient transport of both electrons and lithium ions upon charging/discharging.

2. EXPERIMENTAL SECTION

2.1. Materials. CNTs were synthesized via CVD with ferrocene and 1,2-dichlorobenzene as the catalyst precursor and carbon source, and a quartz sheet as the growth substrate according to the procedure reported elsewhere.[31] SiNW@G nanocables were prepared following a process developed in a previous work.[33] Briefly, the SiNWs were heated to 1050 °C at a rate of 20 °C/min in a horizontal tube furnace under argon/hydrogen (Ar/H_2; 2:1) atmosphere, then 50 sccm CH_4 was introduced into the reaction tube and kept for 5 min. After that, the sample was rapidly cooled to room temperature under the protection of Ar and H_2, thus obtaining silicon nanowire/overlapped graphene sheet core−sheath (SiNW@G) nanocables. To produce SiNW@G-CNT hybrids, SiNW@G nanocables were weighed and dispersed in 50 mL of N-methyl-2-pyrrolidone (NMP) by bath sonication (40 kHz, 200 W) for several minutes. Meanwhile, the CNTs were dispersed in NMP by 30 min of sonication to obtain an initial dispersion with a concentration of 1 mg/mL, which was then diluted serially to 100 mL and sonicated to make the dispersion appear completely free from aggregates by visual inspection. The SiNW@G dispersion was then slowly added into the thus-obtained CNT dispersion under sonication, and then vigorously stirred at room temperature overnight. The resultant suspension was condensed on a rotary evaporator, dropped on the current collector and dried in a laboratory vacuum oven. The thus-deposited hybrids were pressed further and used directly as a LIB working electrode without the addition of any binders, in which the mass loading of active material is set to be 0.3−0.5 mg cm^{-2} by controlling the amount of the used suspension. The weight ratio of CNTs to SiNW@G nanocables could be easily adjusted by changing the relative amount of both dispersions. In a control experiment, SiNW@G nanocables were incorporated with graphene oxide as well to get a SiNW@G@RGO working electrode; the detailed procedure has been reported before.

2.2. Characterizations. The structure and morphology of the samples were investigated by FE-SEM (Hitachi S4800) and FE-TEM (FEI Tecnai G2 20 STWIN and Tecnai G2 F20 U-TWIN). For electrochemical measurements, the as-made working electrodes were assembled into coin-type half cells (CR2032) in an argon-filled glovebox with lithium foil as the counter electrode, porous polypropylene film as the separator, and 1 M $LiPF_6$ in 1:1 (v/v) ethylene carbonate/diethyl carbonate (EC/DEC) as the electrolyte. The cycle-life tests were performed using a CT2001A battery program controlling test system at different current rates within 2−0.02 V voltage range. For each investigated working electrode, the total sample weight was used for setting current rates and calculating specific capacities. EIS measurements were performed using a CHI660D electrochemical station (CH Instrument, Shanghai, China), in the frequency range from 100 kHz to 0.01 Hz with an ac perturbation of 5 mV. In some cases, the electrodes after cycling were dissembled and washed with acetonitrile and dilute HCl for further analysis.

3. RESULTS AND DISCUSSION

The fabrication of SiNW@G-CNT was realized via mixing the dispersions of SiNW@G and CNTs in N-methyl-2-pyrrolidone (NMP) under sonication followed by mechanical stirring (see Experimental Section for more details). The SiNW@G nanocables composed of silicon nanowire cores and overlapped graphene sheaths (see the Supporting Information, Figure S1), with an average diameter of 65 nm and a typical length of more than 50 μm, were produced according to our previously reported procedure,[33] and sponge-like CNTs with a typical diameter of ca. 30 nm and a length of tens of micrometers (see the Supporting Information, Figure S2) were synthesized by a chemical vapor deposition (CVD) growth method.[31] The morphology, structure, and composition of the resultant SiNW@G-CNT hybrid materials were characterized by scanning electron microscopy (SEM), transmission electron microscopy (TEM), and energy-dispersive X-ray spectroscopy (EDX). Figure 2a exhibits a representative SEM image of the SiNW@G-CNT, demonstrating a fibrous structure with interconnected pores up to micrometers and distributing uniformly within the whole hybrid. A higher magnification SEM image (Figure 2b) further discloses that CNTs and SiNW@G nanocables are intertwined with each other, forming a 1D/1D interpenetrating 3D network. This is verified in TEM images (Figure 3a, b), in which SiNW@G nanocables are seen to be homogenously dispersed in the CNT network, and vice versa. This observation is in accord with the ability of the used solvent (e.g., NMP) to disperse both CNTs and SiNW@G nanocables under sonication since it has been used to disperse other carbonaceous nanomaterials (e.g., highly bundled single-

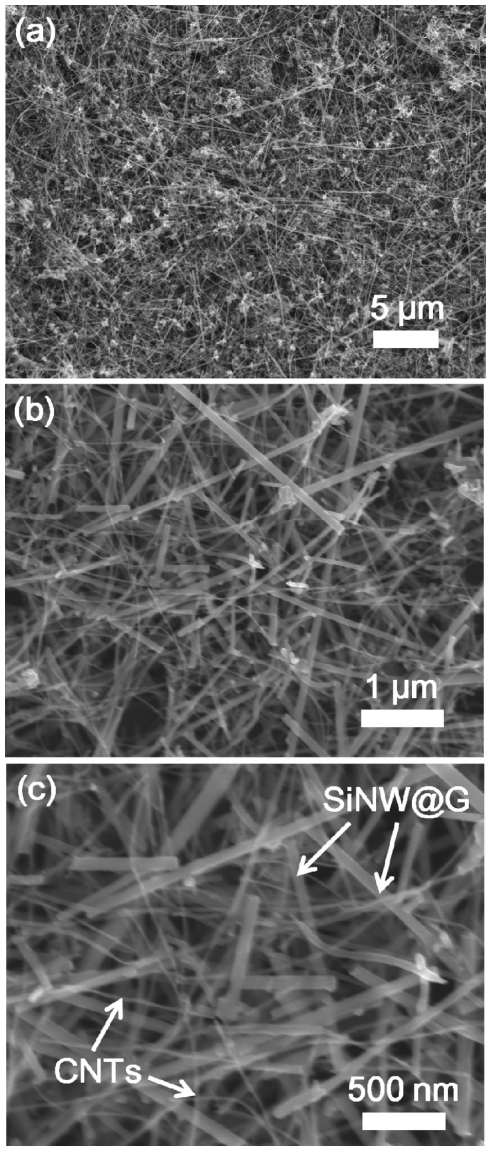

Figure 2. (a–c) SEM images of SiNW@G-CNT with different magnifications.

walled carbon nanotubes).[36] Notably, a small portion of SiNW@G nanocables is shortened in the preparation process of this hybrid as displayed in Figure 3a, which can rather contribute to their facile dispersion in the CNT matrix. The high-resolution TEM image (Figure 3c) reveals that the SiNW@G still consists of a single crystal SiNW core and an irregularly overlapped graphene sheath, which clearly suggests that the used SiNW@G nanocables are quite robust and somewhat resistant to sonication involved in this study. In addition, The EDX analysis shows that the SiNW@G-CNT is mainly composed of Si and C, which is in accord with the presence of both SiNW@G and CNTs in the hybrid, while the small O signal can be related to the oxygen adsorbed on the CNTs during the sample preparation process. In short, the above results suggest the formation of a hierarchical 1D/1D interpenetrating porous network, which is anticipated to exhibit superior lithium storage capability because it provides abundant free spaces (e.g., pores) to accommodate the volume variation of Si, and facilitate the transport of electrons and the diffusion of lithium ions throughout the whole electrode. It should be mentioned that the weight ratio of CNTs to SiNW@G nanocables is adjusted to be around 2:5, considering the preparation of an interconnected hybrid network with minimum addition of CNTs, which can dilute the capacity of the electrode.

The electrochemical properties of SiNW@G-CNT were evaluated by galvanostatic charge/discharge tests based on standard coin-type half cells. Unless otherwise specified, the current density used and specific capacity reported are based on the total SiNW@G-CNT weight. As exhibited in Figure 4a, the SiNW@G-CNT shows competing cycling performance although the capacity decay occurs in the initial cycles presumably due to accidental escape of some excessively short SiNW@G nanocables from the CNT matrix; after 100 cycles, the reversible capacity of SiNW@G-CNT is still as high as 1000 mA h g^{-1}, which is approximately three times that of the commercial graphite anode, and more stable than SiNW@G nanocables assembled into a conventional electrode architecture[33] and also other analogues (e.g., carbon-coated SiNWs mixed with CNTs).[37] This enhancement can be due to the coating of SiNWs with adaptable[33] G sheaths that effectively prevent the direct contact of silicon with electrolyte upon cycling, as well as the use of the porous CNT matrix that better accommodates the volume change of SiNW@G nanocables compared to traditional binders such as polyvinylidene fluoride (PVDF). The superior cycling stability can be further characterized by the preservation of the nanocable/nanotube interpenetrating electrode architecture as confirmed by the TEM image of the sample after running 100 cycles (see the Supporting Information, Figure S3). It should be mentioned that while the first cycle Coulombic efficiency is relatively low (Figure 4a and the Supporting Information, Figure S4), which can be associated with the occurrence of side reactions on the electrode surfaces and interfaces (mainly G sheaths and CNTs) and the SEI formation in the first cycle, the Coulombic efficiency can rapidly increase and stabilize at 99–100% in subsequent cycles, reflecting the stable SEI built on the outside of Si mostly because of the presence of adaptable G sheaths.[33] Another more striking advantage of hybridizing 1D Si/C nanocables with 1D CNTs is evidenced by performing galvanostatic charge/discharge measurements at different current rates. Figure 4b shows the detailed high rate cycling results for the SiNW@G-CNT accompanying those[33] of the SiNW@G@RGO for comparison. Remarkably, the SiNW@G-CNT consistently delivers significantly higher capacity with the increase in the current rate than the SiNW@G@RGO. For example, at a current rate of 4.2 A g^{-1}, the SiNW@G-CNT exhibits a reversible capacity of 1120 mA h g^{-1} compared to only 800 mA h g^{-1} for the SiNW@G@RGO. Even cycling at very high current rates (e.g., 12.6 A g^{-1}), a high capacity of ca. 630 mA h g^{-1} can be obtained with the SiNW@G-CNT electrode on the basis of the total electrode weight, which is still two times that of the SiNW@G@RGO. Apparently, the achieved rate capability is also superior to those of other RGO-incorporated Si-based anodes.[11,30,38] In addition, the capacity retains its nominal value when it is operated back to lower current rates as validated by the case at 4.2 A g^{-1}. Figure 4c displays the voltage profiles of the SiNW@G-CNT cycled at different current rates. Although both G and CNT contribute to the measured capacity, the voltage profiles obtained at different current rates are similar, and in good agreement with the behavior of amorphous silicon which originates from the transformation of crystalline Si in the first charge–discharge

dx.doi.org/10.1021/am402022n | ACS Appl. Mater. Interfaces 2013, 5, 6467–6472

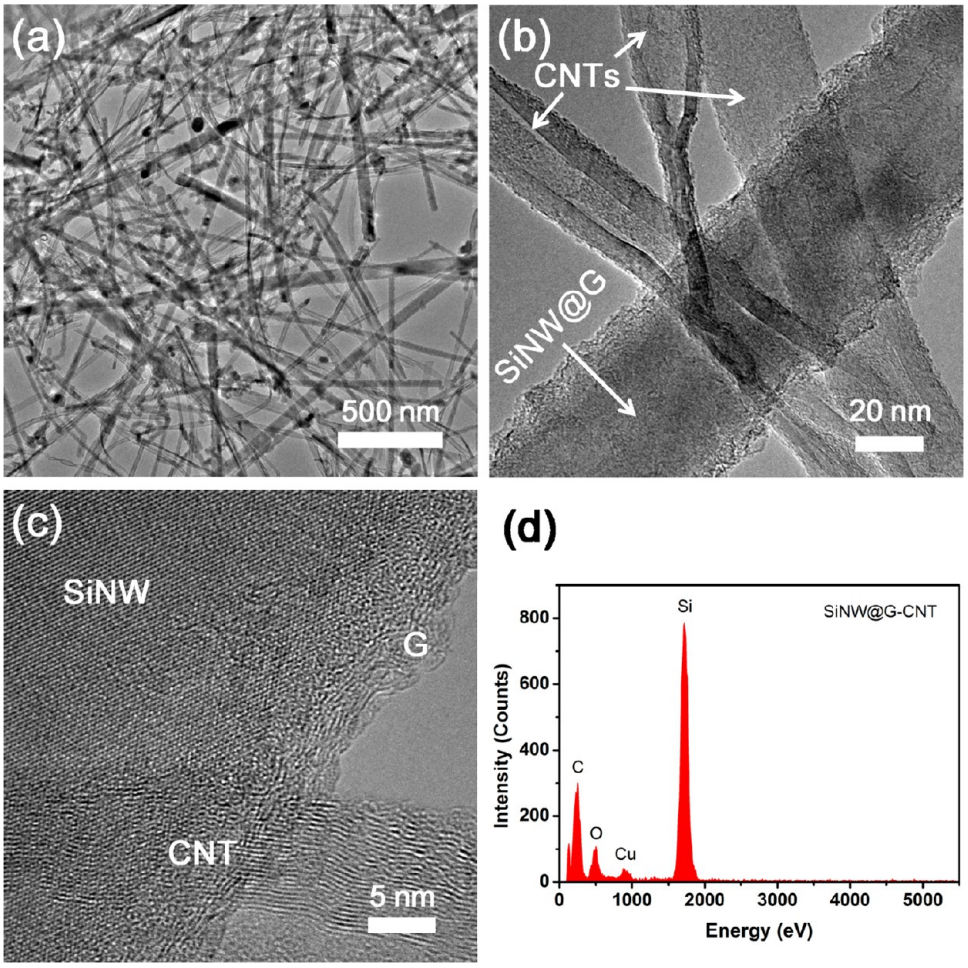

Figure 3. (a, b) TEM images at different magnifications, (c) high-resolution TEM image, and (d) EDX pattern of SiNW@G-CNT.

cycle as implied in Figure S4 in the Supporting Information and discussed elsewhere.[33] The significantly enhanced rate capability of SiNW@G-CNT proves that the 1D/1D nanocable/nanotube hybrid can be used as a good high-rate electrode material for LIBs.

To further understand the origin of the superior lithium-storage performance of SiNW@G-CNT in comparison with SiNW@G@RGO, we performed electrochemical impedance spectroscopy (EIS) measurements of both electrodes after running several cycles at the same current rate. As shown in Figure 4d, the EIS spectra for both electrodes are typically composed of an inclined line in the low-frequency region and a depressed semicircle in the high-frequency region, a behavior that is in good agreement with previously reported impedance spectra of silicon nanowires.[39,40] The inclined line corresponds to the lithium ion diffusion impedance, and the depressed semicircle mainly consists of the interfacial charge transfer impedance at the medium-to-high frequency range although high-frequency SEI film impedance contributes to it. On the one hand, in comparison with that for the SiNW@G@RGO, it is apparent that the Nyquist plot of SiNW@G-CNT shows a shorter diffusion tail in the low frequency region, suggesting that the interconnected open pores or channels in the as-constructed hierarchical 1D/1D hybrid electrodes substantially facilitate the diffusion and transport of lithium ions from the liquid electrolyte into the electrode, thus reducing the lithium ion diffusion resistance.[41] This scenario is consistent with a recent report where the in-plane carbon vacancies created in graphene sheets endow the resultant silicon-graphene electrodes with excellent ionic diffusivity and consequent high rate capacity.[29] On the other hand, the comparison of the semicircle diameter clearly indicates that the charge transfer resistance of SiNW@G-CNT is significantly smaller than that for SiNW@G@RGO. The result implies that the CVD-grown CNTs are more competent to electrically connect the G sheaths of SiNW@G nanocables and thus to afford a conductive network for fast electron transport from/to embedded SiNWs, in comparison with RGO synthesized in this study. Combined with the ability of CNTs to accommodate the volume change of SiNW@G nanocables, as well as the function of G sheaths to effectively prevent the direct contact between SiNWs and electrolyte during cycling and thus alleviate the formation and propagation of the SEI layer similar to that reported previously,[33] the aforementioned features synergistically lead to the remarkably enhanced lithium storage performance of these hierarchical 1D/1D hybrids, especially high rate capability, which is highly desirable for many applications.

4. CONCLUSION

In summary, we have developed a unique binder-free Si-based anode architecture via hybridizing 1D Si/C core−sheath nanocables with 1D carbon nanotubes. The as-obtained hybrid materials exhibit remarkably improved electrochemical performance, especially high rate capability, in comparison with

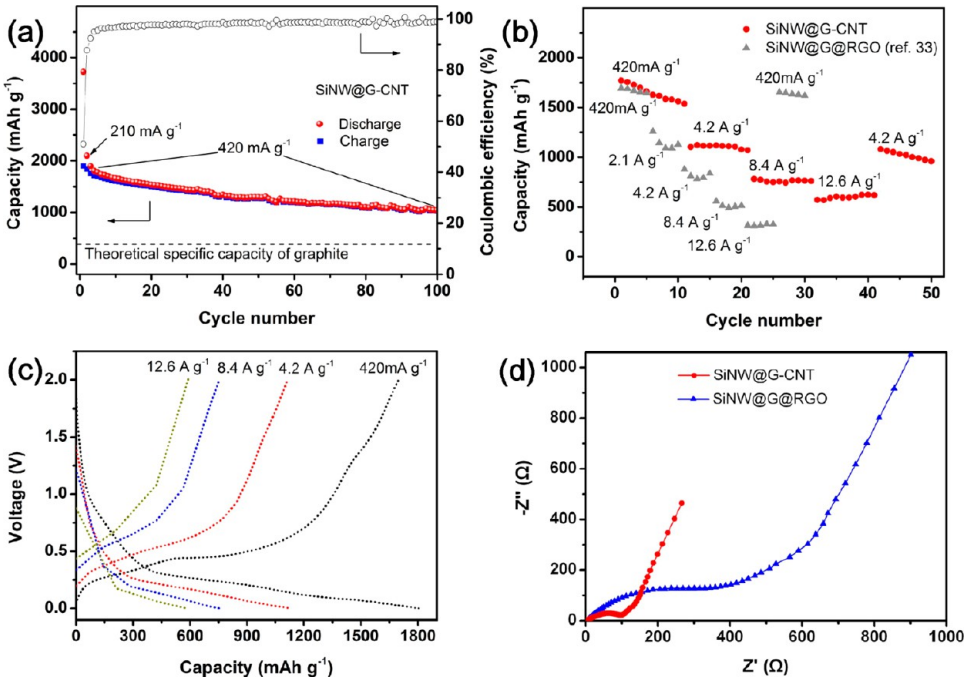

Figure 4. (a) Cycling performance toward 100 cycles at the charge/discharge rate of 210 mA g^{-1} for the first two cycles and then 420 mA g^{-1} for the subsequent cycles. (b) Charge capacities of SiNW@G-CNT in comparison with those of SiNW@G@RGO at various current densities as marked. (c) Voltage profiles for different rates of SiNW@G-CNT in b. (d) EIS spectra of the SiNW@G-CNT in comparison with that of SiNW@G@RGO. All the specific capacities reported and current densities used are based on the total weight of SiNW@G-CNT.

their counterparts such as 2D RGO-hybridized zero-dimensional and/or 1D Si, which can be attributed to their unique hierarchical 1D/1D hybrid structure. As a potential merit, such hierarchical Si/C hybrids can be fabricated in a low-cost and scalable manner, especially given the utilization of silicon nanowires synthesized by other approaches such as metal catalytic etching of commercial silicon wafers.[19] This work provides a novel dimensional strategy toward overcoming the large volume change-related issue of high-capacity anode materials and simultaneously making better LIB electrode architectures with interpenetrating pathways for efficient transport of both electrons and lithium ions. Because the demand for high energy and power density LIBs in applications such as electric vehicles, grids, and renewable energy integration, is ever growing, it would also be of significant interest to extend the electrode formulation demonstrated in this study to other fascinating electrode materials with large volume change and low electronic conductivity.

■ ASSOCIATED CONTENT

Supporting Information

SEM and TEM images of the used SiNW@G nanocables and CNTs; SEM image of the cycled SiNW@G-CNT electrode; Voltage profiles of the first two cycles of the SiNW@G-CNT electrode. This material is available free of charge via the Internet at http://pubs.acs.org.

■ AUTHOR INFORMATION

Corresponding Author

*E-mail: lixl@nanoctr.cn (X.L.); zhilj@nanoctr.cn (L.Z.).

Notes

The authors declare no competing financial interest.

■ ACKNOWLEDGMENTS

Financial support from the National Natural Science Foundation of China (Grants 20973044, 21173057, 21273054), the Ministry of Science and Technology of China (2012CB933400 and 2012CB933403), the Beijing Municipal Science and Technology Commission (Z121100006812003), and the Chinese Academy of Sciences is acknowledged. The authors also acknowledge the kind help of Dr. S. T. Picraux at Los Alamos National Laboratory.

■ REFERENCES

(1) Tarascon, J. M.; Armand, M. *Nature* **2001**, *414*, 359−367.
(2) Taberna, L.; Mitra, S.; Poizot, P.; Simon, P.; Tarascon, J. M. *Nat. Mater.* **2006**, *5*, 567−573.
(3) Armand, M.; Tarascon, J. M. *Nature* **2008**, *451*, 652−657.
(4) Chan, C. K.; Peng, H. L.; Liu, G.; McIlwrath, K.; Zhang, X. F.; Huggins, R. A.; Cui, Y. *Nat. Nanotechnol.* **2008**, *3*, 31−35.
(5) Kang, B.; Ceder, G. *Nature* **2009**, *458*, 190−193.
(6) Szczech, J. R.; Jin, S. *Energy Environ. Sci.* **2011**, *4*, 56−72.
(7) Wu, H.; Cui, Y. *Nano Today* **2012**, *7*, 414−429.
(8) Cao, F. F.; Deng, J. W.; Xin, S.; Ji, H. X.; Schmidt, O. G.; Wan, L. J.; Guo, Y. G. *Adv. Mater.* **2011**, *23*, 4415−4420.
(9) Chen, X. L.; Li, X. L.; Ding, F.; Xu, W.; Xiao, J.; Cao, Y. L.; Meduri, P.; Liu, J.; Graff, G. L.; Zhang, J. G. *Nano Lett.* **2012**, *12*, 4124−4130.
(10) Gohier, A.; Laïk, B.; Kim, K.-H.; Maurice, J.-L.; Pereira-Ramos, J.-P.; Cojocaru, C. S.; Van, P. T. *Adv. Mater.* **2012**, *24*, 2592−2597.
(11) Luo, J. Y.; Zhao, X.; Wu, J. S.; Jang, H. D.; Kung, H. H.; Huang, J. X. *J. Phys. Chem. Lett.* **2012**, *3*, 1824−1829.
(12) Li, X.; Cho, J. H.; Li, N.; Zhang, Y. Y.; Williams, D.; Dayeh, S. A.; Picraux, S. T. *Adv. Energy Mater.* **2012**, *2*, 87−93.
(13) Yi, R.; Dai, F.; Gordin, M. L.; Chen, S.; Wang, D. *Adv. Energy Mater.* **2013**, *3*, 295−300.
(14) Kasavajjula, U.; Wang, C. S.; Appleby, A. J. *J. Power Sources* **2007**, *163*, 1003−1039.

(15) Wu, H.; Chan, G.; Choi, J. W.; Ryu, I.; Yao, Y.; McDowell, M. T.; Lee, S. W.; Jackson, A.; Yang, Y.; Hu, L. B.; Cui, Y. *Nat. Nanotechnol.* **2012**, *7*, 310−315.
(16) Ng, S. H.; Wang, J. Z.; Wexler, D.; Konstantinov, K.; Guo, Z. P.; Liu, H. K. *Angew. Chem., Int. Ed.* **2006**, *45*, 6896−6899.
(17) Kim, H.; Seo, M.; Park, M. H.; Cho, J. *Angew. Chem., Int. Ed.* **2010**, *49*, 2146−2149.
(18) Kim, H.; Cho, J. *Nano Lett.* **2008**, *8*, 3688−3691.
(19) Huang, R.; Fan, X.; Shen, W. C.; Zhu, J. *Appl. Phys. Lett.* **2009**, *95*, 133119.
(20) Chen, H.; Dong, Z.; Fu, Y.; Yang, Y. *J. Solid State Electrochem.* **2010**, *14*, 1829−1834.
(21) Cho, Y. J.; Kim, H. S.; Im, H.; Myung, Y.; Jung, G. B.; Lee, C. W.; Park, J.; Park, M. H.; Cho, J.; Kang, H. S. *J. Phys. Chem. C* **2011**, *115*, 9451−9457.
(22) Yao, Y.; Liu, N.; McDowell, M. T.; Pasta, M.; Cui, Y. *Energy Environ. Sci.* **2012**, *5*, 7927−7930.
(23) Park, M. H.; Kim, M. G.; Joo, J.; Kim, K.; Kim, J.; Ahn, S.; Cui, Y.; Cho, J. *Nano Lett.* **2009**, *9*, 3844−3847.
(24) Hertzberg, B.; Alexeev, A.; Yushin, G. *J. Am. Chem. Soc.* **2010**, *132*, 8548−8549.
(25) Yoo, J.-K.; Kim, J.; Jung, Y. S.; Kang, K. *Adv. Mater.* **2012**, *24*, 5452−5456.
(26) Deng, J. W.; Ji, H. X.; Yan, C. L.; Zhang, J. X.; Si, W. P.; Baunack, S.; Oswald, S.; Mei, Y. F.; Schmidt, O. G. *Angew. Chem., Int. Ed.* **2013**, *52*, 2326−2330.
(27) Kovalenko, I.; Zdyrko, B.; Magasinski, A.; Hertzberg, B.; Milicev, Z.; Burtovyy, R.; Luzinov, I.; Yushin, G. *Science* **2011**, *334*, 75−79.
(28) Wang, J. Z.; Zhong, C.; Chou, S. L.; Liu, H. K. *Electrochem. Commun.* **2010**, *12*, 1467−1470.
(29) Zhao, X.; Hayner, C. M.; Kung, M. C.; Kung, H. H. *Adv. Energy Mater.* **2011**, *1*, 1079−1084.
(30) Wang, B.; Li, X.; Luo, B.; Jia, Y.; Zhi, L. *Nanoscale* **2013**, *5*, 1470−1474.
(31) Hu, L. B.; Wu, H.; Gao, Y. F.; Cao, A. Y.; Li, H. B.; McDough, J.; Xie, X.; Zhou, M.; Cui, Y. *Adv. Energy Mater.* **2011**, *1*, 523−527.
(32) Evanoff, K.; Khan, J.; Balandin, A. A.; Magasinski, A.; Ready, W. J.; Fuller, T. F.; Yushin, G. *Adv. Mater.* **2012**, *24*, 533−537.
(33) Wang, B.; Li, X.; Zhang, X.; Luo, B.; Jin, M.; Liang, M.; Dayeh, S. A.; Picraux, S. T.; Zhi, L. *ACS Nano* **2013**, *7*, 1437−1445.
(34) Long, J. W.; Dunn, B.; Rolison, D. R.; White, H. S. *Chem. Rev.* **2004**, *104*, 4463−4492.
(35) Rolison, D. R.; Long, R. W.; Lytle, J. C.; Fischer, A. E.; Rhodes, C. P.; McEvoy, T. M.; Bourga, M. E.; Lubers, A. M. *Chem. Soc. Rev.* **2009**, *38*, 226−252.
(36) Ausman, K. D.; Piner, R.; Lourie, O.; Ruoff, R. S.; Korobov, M. *J. Phys. Chem. B* **2000**, *104*, 8911−8915.
(37) Chan, C. K.; Patel, R. N.; O'connell, M. J.; Korgel, B. A.; Cui, Y. *ACS Nano* **2010**, *4*, 1443−1450.
(38) Zhou, X.; Yin, Y.-X.; Wan, L.-J.; Guo, Y.-G. *Adv. Energy Mater.* **2012**, *2*, 1086−1090.
(39) Ruffo, R.; Hong, S. S.; Chan, C. K.; Huggins, R. A.; Cui, Y. *J. Phys. Chem. C* **2009**, *113*, 11390−11398.
(40) Chen, X. L.; Gerasopoulos, K.; Guo, J. C.; Brown, A.; Ghodssi, R.; Culver, J. N.; Wang, C. S. *Electrochim. Acta* **2011**, *56*, 5210−5213.
(41) Liu, Y. H.; Zhang, W.; Zhu, Y. J.; Luo, Y. T.; Xu, Y. H.; Brown, A.; Culver, J. N.; Lundgren, C. A.; Xu, K.; Wang, Y.; Wang, C. S. *Nano Lett.* **2013**, *13*, 293−300.